RSC Advances

PAPER

View Article Online
View Journal | View Issue

Cite this: *RSC Adv.*, 2026, **16**, 21277

Efficient electrocatalytic water splitting performance of an $SrTiO_3$/g-C_3N_4 composite for hydrogen evolution in an acidic medium

Leena Baskar,[a] Divyadharshini Satheesh,[a] Paul Joseph Daniel,[b] Vijayarangamuthu Kalimuthu[c] and Kovendhan Manavalan *[a]

Water splitting is a research field that possesses a high scope for the generation of non-polluting and sustainable energy. In this study, an $SrTiO_3$/g-C_3N_4 heterostructure composite is fabricated to boost the catalytic efficacy for the HER applications. The $SrTiO_3$/g-C_3N_4 heterostructure composite was prepared *via* a hydrothermal technique by combining strontium titanate ($SrTiO_3$) nanopowders with 2D graphitic carbon nitride (g-C_3N_4). The formation of the composite heterostructure between $SrTiO_3$ and g-C_3N_4 was confirmed using XRD, SEM, and UV and Raman spectroscopies. The synergy between $SrTiO_3$ and g-C_3N_4 played a key role in enhancing the catalytic efficacy. By combining the unique aspects of $SrTiO_3$ and g-C_3N_4, the fabricated heterostructure composite achieved a low overpotential of 321 mV and a Tafel slope of 192 mV dec^{-1}, indicating improved HER activity and thereby making it an effective catalyst for the hydrogen evolution reaction. The stability of the heterostructure composite was explored for prolonged reaction periods, and by using this composite, hydrogen generation was realized in a sustainable and efficient manner. This strategy is a promising approach to clean and renewable hydrogen generation.

Received 12th February 2026
Accepted 7th April 2026

DOI: 10.1039/d6ra01249c

rsc.li/rsc-advances

1. Introduction

The search for sustainable energy options is accelerated by the growing demand for clean and renewable energy on a global scale. Due to its enormous energy density and zero carbon emissions when in use, hydrogen (H_2) has become one of the most promising sources of energy.[1] One of the most effective and environmentally friendly routes for producing hydrogen is electrochemical water splitting, which is composed of two important half-reactions: the hydrogen evolution reaction (HER) at the cathode and the oxygen evolution reaction (OER) at the anode.[2] The hydrogen evolution reaction (HER) is crucial for producing hydrogen gas, and it occurs by reducing protons in acidic conditions or by reducing water molecules in alkaline conditions, ultimately liberating hydrogen.[3,4] Platinum (Pt)-based catalysts have shown enhanced performance for the HER because of their low overpotentials and high exchange current densities.[5,6] Nevertheless, the high cost and scarcity of platinum hinder their scalability for real-time applications. This has led to intensive research into earth-abundant, low-cost alternative materials, such as transition metal compounds, metal-free catalysts, and heterostructured electrocatalysts.[7]

Strontium titanate ($SrTiO_3$) has an ideal cubic perovskite-like unit cell of the ABO_3 oxide system, wherein the Sr^{2+} and Ti^{4+} ions constitute the A and B sites, respectively. Nevertheless, an ideal perovskite-like STO shows lattice distortion at different levels, which determines the crystal field and, eventually, the dipole and electronic band structures. This lattice distortion also influences the photoinduced charge carrier aspects of STO, which is crucial for photocatalytic steps like excitation, transfer, and redox reactions.[8,9] Perovskite-type strontium titanate ($SrTiO_3$)[10] has attracted attention in photocatalysis and electrocatalysis due to its chemical stability, tunable electronic structure, and good conductivity. $SrTiO_3$ exhibits suitable conduction and valence band positions that can support the HER under acidic conditions. However, its practical application is often limited by its wide bandgap (~3.61 eV), which restricts visible light absorption, and by its relatively low intrinsic catalytic activity. To overcome these limitations, graphitic carbon nitride (g-C_3N_4) has been explored as a supporting material.[11–13] g-C_3N_4 is a metal-free polymeric semiconductor with a narrower bandgap (~2.86 eV), enabling better visible-light absorption. It also possesses a layered structure, good chemical stability, and potential active sites for the HER. Often, g-C_3N_4 alone suffers from fast electron–hole recombination and limited charge mobility.[14,15]

By combining $SrTiO_3$ with g-C_3N_4, a heterojunction composite can be formed, which synergistically enhances the

[a]*Department of Physics and Nanotechnology, SRM Institute of Science and Technology, Kattankulathur, Chengalpattu-603203, Tamil Nadu, India. E-mail: mkovendhan@gmail.com*

[b]*Department of Physics, National Institute of Technology-Warangal, Telangana State-506004, India*

[c]*Department of Physics, Pondicherry University, Kalapet, Pondicherry-605014, India*

overall electrocatalytic performance.[16,17] The characteristics of the heterostructure composite facilitate improved charge separation, extend the light absorption range, and increase the number of active sites. The interaction of $SrTiO_3$ with g-C_3N_4 at the interface helps in suppressing recombination losses and boosts catalytic efficiency under electrochemical conditions.[18,19] In this context, the $SrTiO_3$/g-C_3N_4 composite presents a promising strategy for developing efficient and sustainable HER electrocatalysts. This work aims to investigate the synthesis, characterization, and HER performance of the $SrTiO_3$/g-C_3N_4 composite and to elucidate the synergistic mechanisms contributing to its enhanced catalytic behavior.[20,21]

2. Materials and experimental methods

Titanium butoxide ($Ti(OBu)_4$), strontium nitrate ($Sr(NO_3)_2$), and sodium hydroxide (NaOH) were procured from Sisco Research Laboratories Pvt. Ltd, and melamine (99%) was obtained from Sigma-Aldrich. All chemicals and ethylene glycol solvent were used as procured without any further purification.

2.1. Synthesis of $SrTiO_3$

5 mmol of $Ti(OBu)_4$ was dissolved in 25 mL of ethylene glycol by stirring. Following the addition of 5 mL of 5 M NaOH solution, 10 mL of 0.5 M $Sr(NO_3)_2$ solution was added to the solution. After mixing for 10 min, the contents were transferred into a 50 mL Teflon-lined stainless steel autoclave and treated at 180 °C for 24 h. The resultant solid particles were collected by centrifuging with deionized water and ethanol, respectively. The solution is then dried at 70 °C for 12 h, and a white colour precipitate confirmed the formation $SrTiO_3$.[22]

2.2. Preparation of the $SrTiO_3$/g-C_3N_4 composite

g-C_3N_4 was prepared by treating melamine at 550 °C in a box furnace for 4 h, and a yellow-colored powder was obtained. The preparation of the $SrTiO_3$/g-C_3N_4 heterostructure involved combining the prepared $SrTiO_3$ nanoparticles and g-C_3N_4 sheets by ultrasonication.[23] Heterostructures with different compositions of g-C_3N_4 (1, 3 and 5%) were dispersed in water, followed by the addition of $SrTiO_3$ powders and then ultrasonicated for 1 h and mixed for 30 min. Finally, the mixture was treated at 80 °C for 12 h to obtain 1%, 3% and 5% g-C_3N_4-incorporated samples. The final product was obtained for different concentrations and are named as ST, GCN, S1G, S3G, and S5G.[24]

2.3. Mechanism of the HER under acidic conditions

The hydrogen evolution reaction (HER) is a process that leads to the generation of hydrogen gas at the surface of the working electrode. The chemical pathway varies depending on whether the electrolyte is acidic or alkaline. Under acidic conditions, the HER mechanism begins with the Volmer step (eqn (1)), which involves the electrochemical discharge of a proton. This is followed by either the Tafel reaction (eqn (2)), the Heyrovsky reaction (eqn (3)) or a combination of both.[25]

$$H_3O^+ + e^- + M \rightarrow H_{ads} + H_2O \text{ (Volmer)} \quad (1)$$

$$H_{ads} + H_{ads} \rightarrow H_2 \text{ (Tafel)} \quad (2)$$

$$H_{ads} + H_3O^+ + e^- \rightarrow H_2 + H_2O \text{ (Heyrovsky)} \quad (3)$$

In the Volmer–Heyrovsky mechanism, the initial step corresponds to proton adsorption (eqn (1)), followed by hydrogen evolution *via* the Heyrovsky step (eqn (3)). Here, an adsorbed hydrogen atom (H*) reacts with a proton from the acidic medium and an electron from the surface of the electrode to form molecular hydrogen (H_2) and water. This pathway typically dominates when the surface coverage of adsorbed hydrogen is low, allowing for efficient electron transfer and product formation.

The Tafel curve, derived from the Tafel relation:

$$\eta = a + b\log(j) \quad (4)$$

illustrates a linear behaviour between the overpotential (η), Tafel slope (b), and logarithm of the current density ($\log|j|$). This plot is commonly used to evaluate catalytic performance and to identify the possible HER mechanism. A lower Tafel slope indicates that the electrocatalyst can achieve higher current densities at lower overpotentials, suggesting more efficient charge transfer kinetics and enhanced HER activity.

Cyclic voltammetry (CV) measurements are performed for a minimum of 30 cycles to assess the catalytic efficacy of the HER process. These measurements were executed at a scan rate of 5 mV s^{-1} within a potential range of 0 to −1 V (*vs.* the Reversible Hydrogen Electrode, RHE). The Tafel slope was measured from linear sweep voltammetry (LSV) experiments at a consistent scan rate of 5 mV s^{-1}. Electrochemical Impedance Spectroscopy (EIS) measurements were also carried out to analyze the charge transfer behavior of the synthesized catalyst.[26]

3. Results and discussion

3.1. X-ray analysis

The phase and crystal structure of pure $SrTiO_3$, g-C_3N_4 and $SrTiO_3$/g-C_3N_4 (1, 3 and 5% of g-C_3N_4) composites measured and analysed using a PANalytical Xpert-Pro instrument are shown in Fig. 1a. The tetragonal phase of $SrTiO_3$ with space group *Pm3m* matches with JCPDS file no. 35-0734. The small peak observed at 25.3° belongs to the TiO_2 anatase phase, originating from the precursor used to prepare $SrTiO_3$.[22] The XRD pattern of g-C_3N_4 shows two broad peaks at $2\theta = 13.2°$ and 27.3° that are attributed to graphitic carbon nitride with crystallographic planes (100) and (002). The first peak is due to the in-plane alignment with a repeated periodicity between the triazine or heptazine, while the latter is ascribed to the planar graphitic interlayer periodicity of g-C_3N_4.[27] Compared to the sharp diffraction peaks of $SrTiO_3$, the peaks of g-C_3N_4 are broader and less sharp, which may be due to the smaller size

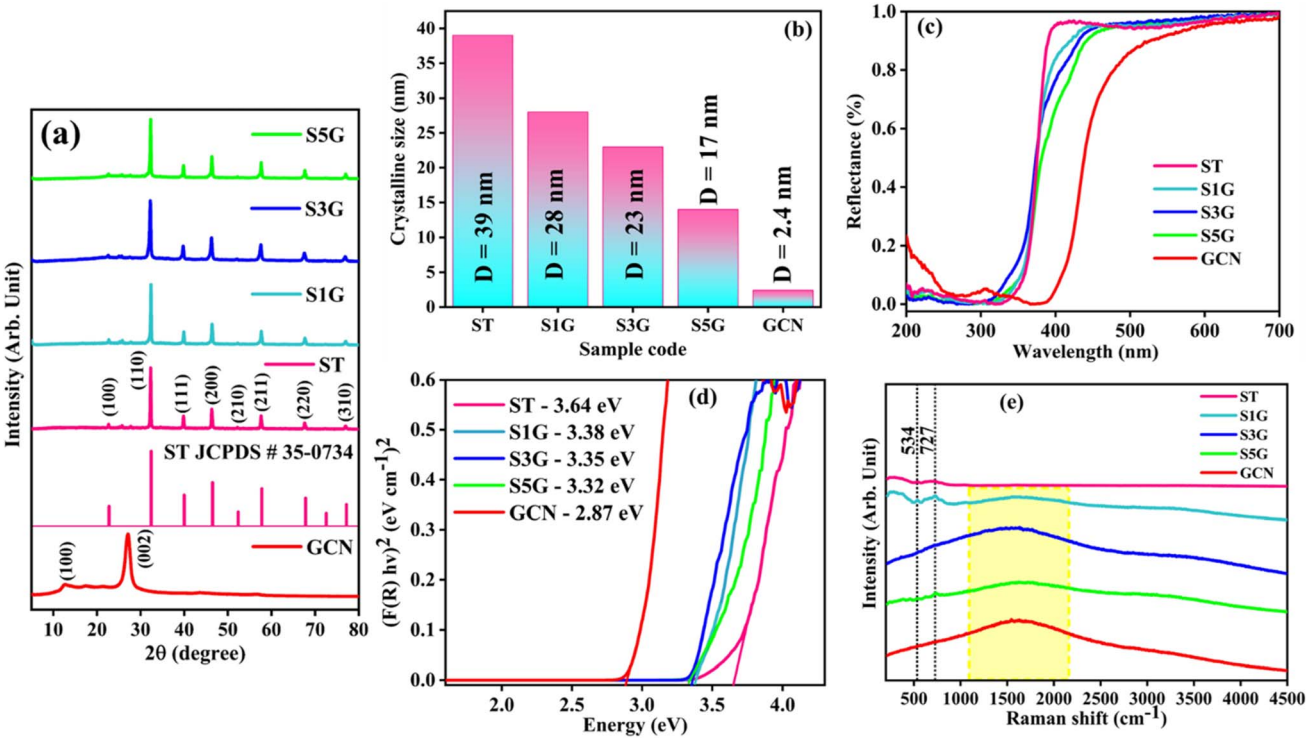

Fig. 1 (a) X-ray diffraction plots, (b) calculated crystallite size using Scherrer relation, (c) UV-vis diffuse reflectance spectra, (d) bandgap obtained from the Kubelka–Munk relation fitting and (e) Raman spectra of the synthesized pure $SrTiO_3$, g-C_3N_4 and $SrTiO_3$/g-C_3N_4 composite samples.

and lower crystallinity of g-C_3N_4. No diffraction maxima of g-C_3N_4 were observed in the $SrTiO_3$/g-C_3N_4 composite because of the low mass concentration; however, it is confirmed by Raman analysis and discussed in the upcoming sections. The average crystallite size estimated using Scherrer's relation was found to decrease systematically due to the incorporation of g-C_3N_4 with $SrTiO_3$, as shown in Fig. 1b.

3.2. UV-vis DRS spectroscopic analysis

The optical characteristics of $SrTiO_3$, g-C_3N_4 and the resultant composites with different mass ratios were assessed by UV-vis diffuse reflectance spectroscopy (DRS). The reflectance spectra of all the prepared samples show a decrease in reflectance after the incorporation of g-C_3N_4 in $SrTiO_3$, indicating light absorption ability of the heterostructure samples.[28] The bandgap was estimated using the Kubelka–Munk function, and it reveals the incorporation of g-C_3N_4 in $SrTiO_3$ to decrease the bandgap of composites because of the interfacial heterojunction formation, electronic interactions, defect states, and synergistic optical properties of the composite materials, making it suitable for electrocatalytic applications.[29]

3.3. Raman spectra analysis

The Raman spectra of hydrothermally synthesized $SrTiO_3$ with an observed band at 534 cm^{-1} are attributed to the first order Ti–O–Ti bending mode with very low intensity and their wavenumbers are assigned to the TO_4 phonon, respectively.[30] The 727 cm^{-1} band is due to second order Ti–O stretching modes in $SrTiO_3$ that arise from the breaking of the crystal symmetry. The broad maxima in the 1000–2400 cm^{-1} region in the Raman spectra of g-C_3N_4 are due to the combination of structural and vibrational factors. Unlike pristine graphite, the incorporation of nitrogen creates structural defects and chemical heterogeneity, resulting in the inhomogeneous widening of vibrational modes.[31] This broad maxima is a result of the overlap of several vibrational contributions, including the G-band (~1570 cm^{-1}), which is related to in-plane stretching of sp^2-bonded carbon atoms, and the d-band (~1350 cm^{-1}), which is linked to structural disorder. In the S5G sample, the contribution of g-C_3N_4 is clearly seen with $SrTiO_3$ (Fig. 1e), confirming the formation of composites.[32]

3.4. X-ray photoelectron spectroscopy

X-ray photoelectron spectroscopy (XPS) for $SrTiO_3$ with 5% of g-C_3N_4 (S5G) was performed. The XPS survey spectrum of S5G in Fig. 2a indicates the presence of constituent Sr, Ti, O, C and N elements. The Sr 3d peaks with binding energies of 132.9 eV and 134.72 eV with two deconvoluted curves, as shown in Fig. 2b, are ascribed to Sr $3d_{5/2}$ and Sr $3d_{3/2}$ levels, respectively.[11] For Ti 2p, binding energies indexed at 458.5 eV and 464.2 eV are ascribed to the Ti $2p_{3/2}$ and Ti $2p_{1/2}$ levels, respectively, as shown in Fig. 2c. The peak at 458.5 eV is related to Ti^{4+} in the octahedron.[33] The O 1s spectrum shows two peaks at 529.5 eV and 531.2 eV in Fig. 2d that are attributed to lattice oxygen (O_L) and surface hydroxyl groups (OOH), respectively.[34] The N 1s spectrum shows a peak at 389.9 eV corresponding to the pyridyl type linked to the sp^2 hybridized nitrogen (C=N–C) in the heptazine ring, and the peak at 400.6 eV corresponds to the pyrrolic type

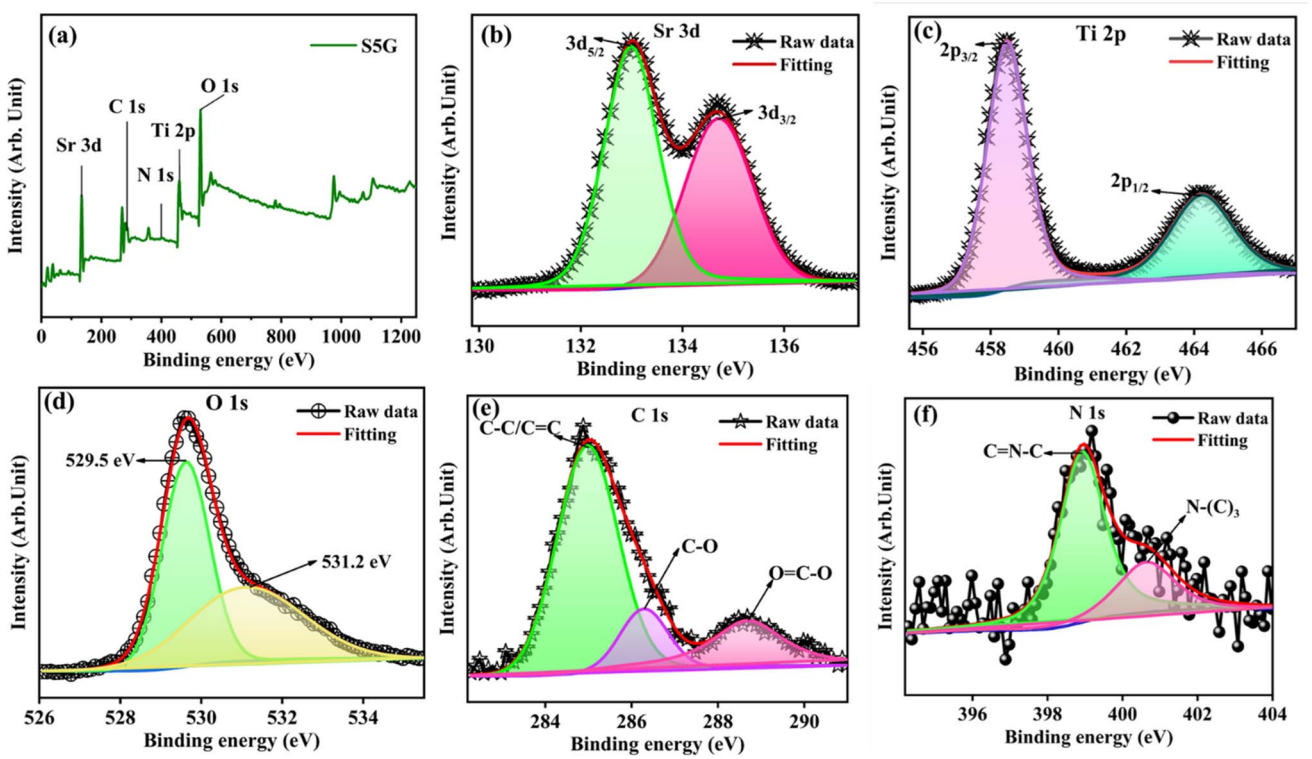

Fig. 2 (a) XPS survey spectra of the S5G heterostructure sample, and the core level spectra of (b) Sr 3d, (c) Ti 2p, (d) O 1s, (e) C 1s and (f) N 1s.

related to the sp^3 hybridized tertiary nitrogen (N–$(C)_3$) (Fig. 2f). The C 1s spectrum in Fig. 2e exhibits peaks at 285 eV, 286.3 eV and 288 eV, ascribed to the band energies of C–C/C═C, C–O and O═C–O, respectively.[33]

3.5. Surface morphological and compositional studies

The SEM image of $SrTiO_3$ reveals the formation of a tetragonal structure in Fig. 3a. Fig. 3b indicates the successful formation of the graphitic stacking structure.[10,35] The arrangement of $SrTiO_3$ is evenly distributed across the g-C_3N_4 surface, as shown in Fig. 3c–e. High-resolution transmission electron microscopy (HR-TEM) images of $SrTiO_3$, g-C_3N_4, $SrTiO_3$ (with 1, 3, and 5% of g-C_3N_4) are presented in Fig. 4a–e. The TEM image of $SrTiO_3$ reveals tetragonal morphology and g-C_3N_4 shows the formation of a stacked sheet-like layer, indicating the formation of a 2D structure. Fig. 4c–e vividly shows the formation of the composite, tetragonal $SrTiO_3$, along with the layer of graphitic carbon nitride.[27,36] The SAED image of the S5G composite in Fig. 4f shows the (002) plane of g-C_3N_4 and (111), (110) and (101) planes of $SrTiO_3$, confirming the formation of the composite. The TEM-EDX spectrum of S5G in Fig. 4g shows the presence of Sr, Ti, O, C and N elements in the composites in the desired ratio.[37]

4. Electrochemical studies

Electrochemical measurements were executed in a three-electrode setup utilizing an OrigaMaster 5 workstation. The counter electrode is a platinum (Pt) wire, and a saturated silver/silver chloride (Ag/AgCl) electrode served as reference with a potential of approximately 0.197 V. The observed decrease in bandgap in the $SrTiO_3$/g-C_3N_4 composites arises from the interfacial heterojunction formation, electronic interactions, defect states, and synergistic optical properties of the composite materials. As an acidic electrolyte, a 0.5 molar solution of sulfuric acid (H_2SO_4) was used. For the working electrode, the composite ($SrTiO_3$/g-C_3N_4) was coated over a 5 × 5 cm size of carbon cloth. Before this coating, the carbon cloth was subjected to an intense cleaning procedure, comprising numerous washes with ethanol and sonication for 60 minutes.[25,38] For making the catalyst slurry, 3 mg of the respective sample (ST, S1G, S3G, S5G, and GCN) was mixed with deionized water (700 μL), ethanol (200 μL), and Nafion (50 μL). This slurry was ultrasonicated for 60 minutes to attain a homogeneous ink. A 34.5 μL of the prepared ink was drop-casted onto one side of the carbon cloth, resulting in a working electrode with a surface area of 0.25 cm^2. Finally, the carbon cloth cast with the $SrTiO_3$/g-C_3N_4 ink was dried at ambient temperature for 24 hours. For the sake of comparison, a bare carbon cloth was used for all the electrochemical measurements.[26,32]

4.1. Linear sweep voltammetry

Linear sweep voltammetry (LSV) curves were measured at a scan rate of 5 mV s^{-1} in order to assess the HER activity. The working electrode potential is linearly swept over time to measure the variation in current with applied potential in order to assess the catalytic activity of materials. The achieved overpotential values at 10 mA cm^{-2} for BARE CC, ST, GCN, S1G, S3G, and S5G were found to be 549, 439, 376, 368, 399, and 321 mV, respectively, as

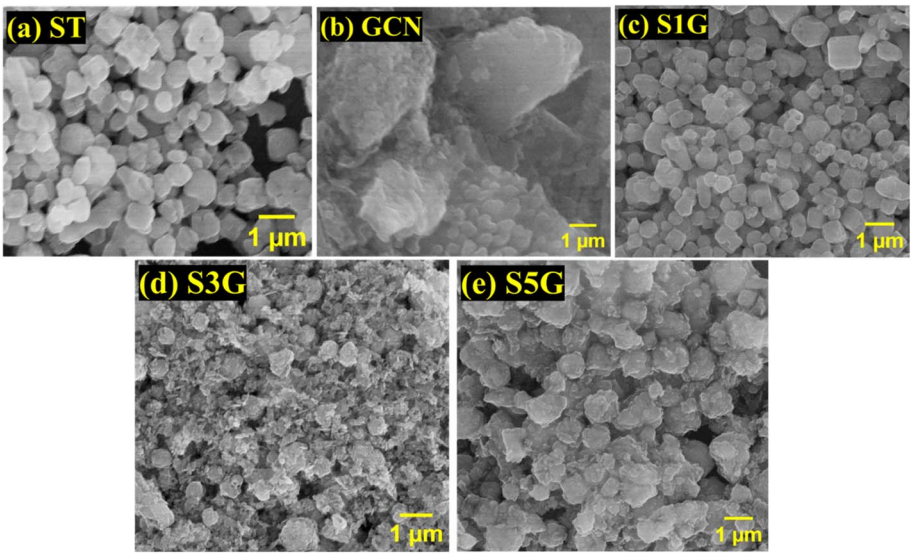

Fig. 3 (a–e) SEM images showing the morphology of the ST, GCN, S1G, S3G, and S5G samples.

shown in Fig. 5a. In general, the low overpotential value for the S5G composite indicates that enhancing the composites ratio will lead to increased current density.[39] In Fig. 5b, the zoomed-in plot of LSV at 10 mA cm^{-2} is shown.

4.2. Tafel analysis

Tafel curves were obtained from the LSV plot as depicted in Fig. 5c. The Tafel slopes of BARE CC, ST, GCN, S1G, S3G, and S5G were determined to be 336, 254, 289, 225, 234, and 192 mV dec^{-1}, respectively. Among them, the S5G sample exhibited the lowest Tafel slope of 192 mV dec^{-1}, indicating enhanced catalytic efficiency.[11] A lower Tafel slope suggests that the catalyst can achieve higher current densities with lower overpotentials. Since catalysts with lower Tafel slopes require low additional energy to accelerate the reaction rate, they are considered more efficient in promoting the hydrogen evolution reaction (HER). The bar graph comparison for pure components and composites is depicted in Fig. 5d.

4.3. Chronoamperometric test

The stability of the $SrTiO_3$ electrocatalyst with 5% g-C_3N_4 is explored by chronoamperometry test (CA) at relevant potential values using the LSV experiment for a duration of 12 h. Fig. 5e shows the stability of the S5G catalyst from the cathodic polarization curve scanned at a rate of 50 mV s^{-1}.[40,41] The curve indicates a slight increment from the initial current density over a 12 h period, indicating the enhanced stability of the heterostructure catalyst S5G in the acidic medium. Therefore, $SrTiO_3$

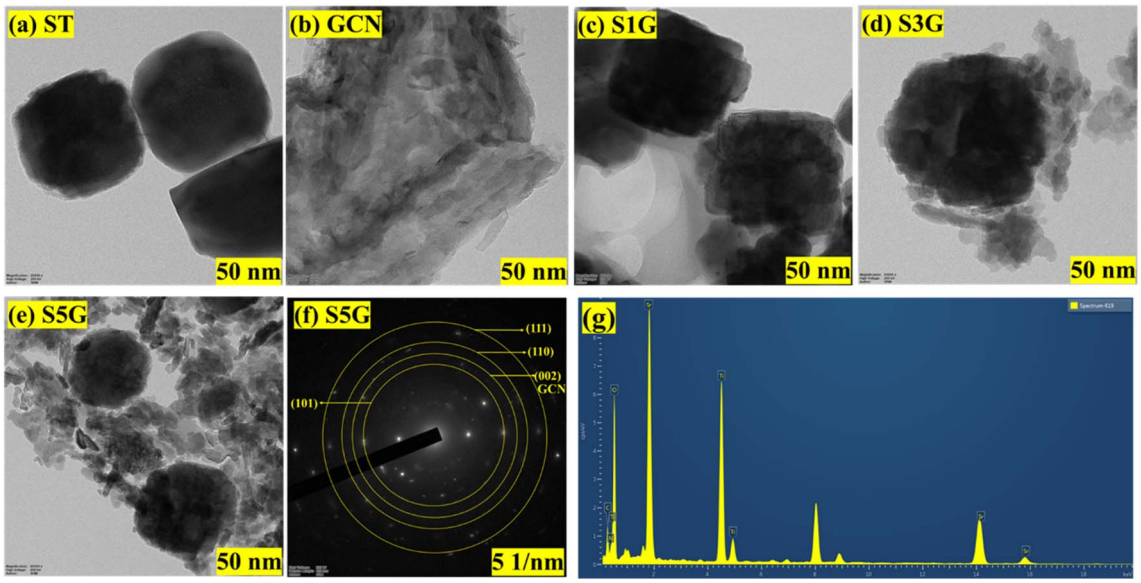

Fig. 4 (a–e) TEM images of ST, GCN, S1G, S3G and S5G, and (f) SAED pattern and (g) TEM-EDX spectrum of the selected S5G composite.

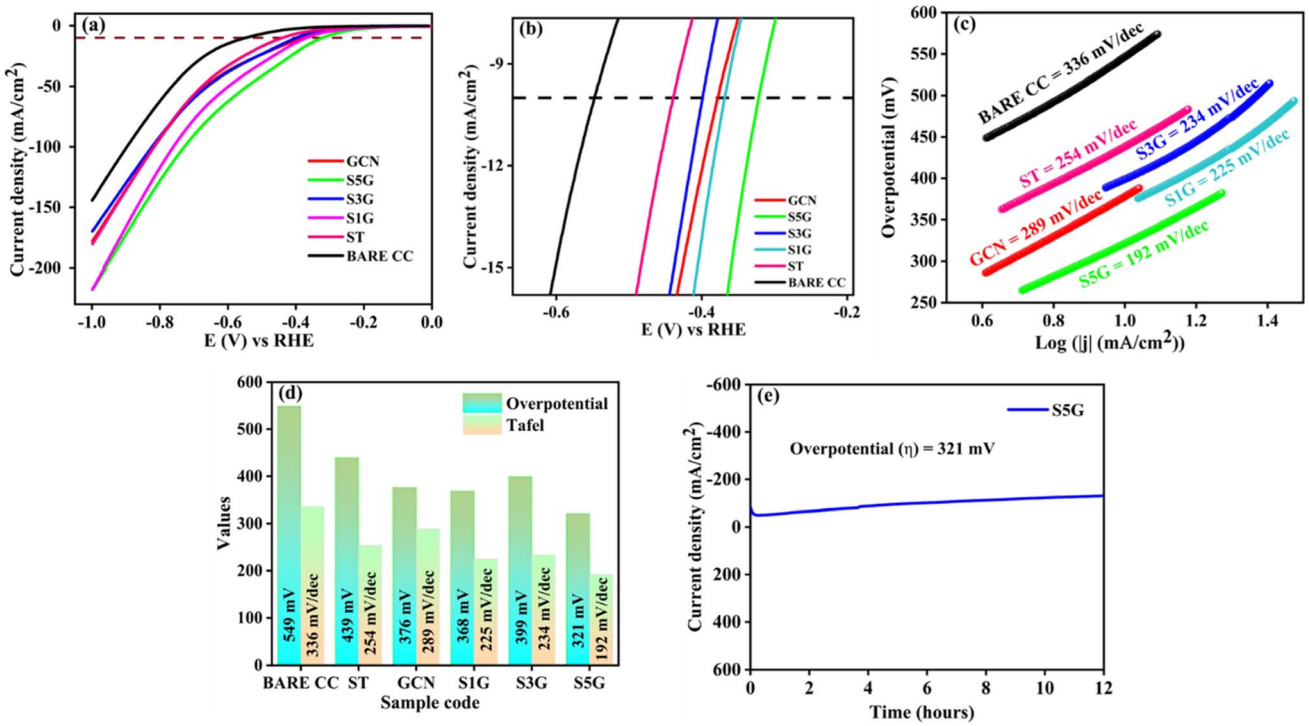

Fig. 5 (a) Linear sweep voltammetry (LSV) curves, (b) zoomed-in plot of LSV curves at −10 mA cm^{-2}, (c) Tafel plots, (d) comparison bar graph of overpotential and Tafel slopes and (e) chronoamperometric analysis of the optimal S5G composite catalyst.

with 5% g-C_3N_4 ensured that the composite can significantly elevate the electrochemical efficacy for the HER process in the acidic medium.

4.4. Electrochemical impedance spectroscopy

The Nyquist curves obtained from electrochemical impedance spectroscopy (EIS) yield details about the charge transfer

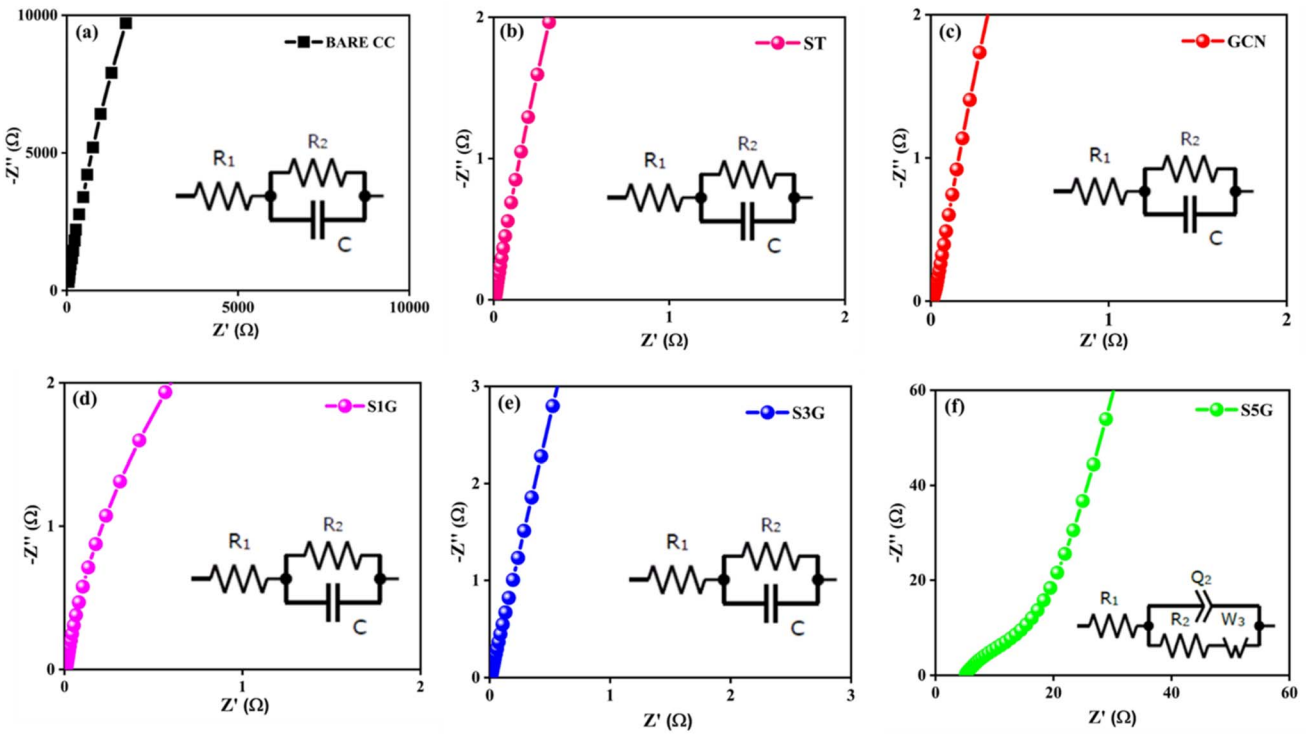

Fig. 6 Electrochemical impedance spectroscopy (EIS) Nyquist plots of the (a) BARE CC, (b) ST, (c) GCN, (d) S1G, (e) S3G and (f) S5G samples, along with their respective equivalent circuits.

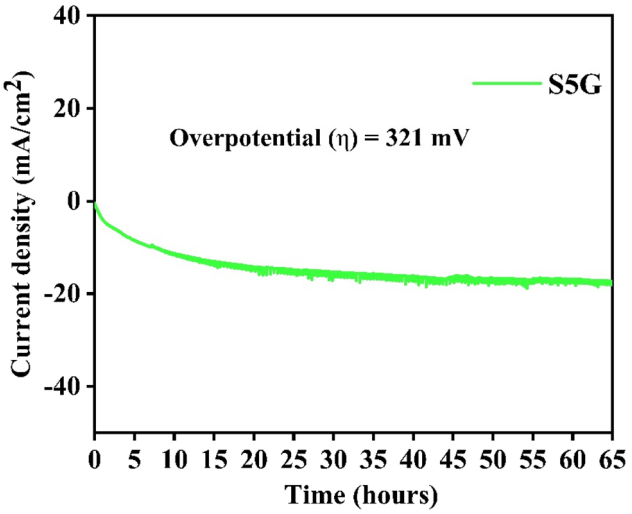

Fig. 7 Chronoamperometric test of the optimal S5G composite catalyst.

kinetics at the interfaces. For pure ST, S1G, S3G and BARE CC (Fig. 6a–e), the equivalent circuits are also shown in the insets of Fig. 6, as derived from eqn (5),

$$Z = R_1 + (R_2/C) \quad (5)$$

where R_1 represents the solution resistance, R_2 denotes the charge-transfer resistance, and C corresponds to the double-layer capacitance. The EIS curve of S5G presented in Fig. 6f corresponds to the following equation (eqn (6)),

$$Z = R_1 + Q_2/(R_2 + W_3) \quad (6)$$

where Q_2 is for the constant phase element, R_2 is the charge-transfer resistance and W_3 represents the Warburg diffusion element, indicating diffusion-related processes in the electrode.

EIS measurements were performed in the frequency ranging from 100 kHz to 1 Hz. Among all the samples, S5G exhibits the smallest semicircle in the Nyquist plot, indicating the lowest charge transfer resistance (R_{ct}). This ensures that the S5G composite is optimal, as it shows a minimized R_{ct} value and more efficient charge transfer at the electrode–electrolyte interface.[26]

4.5. Long-term stability

The stability of the electrocatalyst $SrTiO_3$ with 5% g-C_3N_4 is explored by a chronoamperometry test (CA) as shown in Fig. 7 at a relevant potential value from the LSV experiment for a duration of 65 h. The current density shows a decrease to around ~10 mA cm^{-2} for the first few hours, which is attributed to the stabilization of active sites. Following this, the current density remains nearly constant throughout the testing time, maintaining a near constant current density at around ~18 mA cm^{-2}, indicating significant electrochemical durability for 65 h. The overpotential value of 321 mV ensures better HER activity. The sample S5G possesses good stability for possible long-term hydrogen evolution applications.

5. Conclusion

The $SrTiO_3$/g-C_3N_4 heterostructure sample was optimized to boost the hydrogen evolution reaction (HER) activity. Electrochemical analysis for HER performance in an acidic environment demonstrated improved efficiency, with the heterostructure composite S5G achieving a low overpotential of 321 mV, Tafel slope of 192 mV dec^{-1} and a significant stability of 65 h. The integration of g-C_3N_4 with $SrTiO_3$ significantly improves HER activity compared to the individual pure $SrTiO_3$ and g-C_3N_4 components, making it a viable material for sustainable and efficient hydrogen generation. The synergy between $SrTiO_3$ and g-C_3N_4 in the heterostructure sample enhances the electrochemical active surface area, leading to more efficient charge transfer for effective hydrogen production. Overall, the composite comprising $SrTiO_3$ with 5% g-C_3N_4 stands out as a promising candidate for the development of sustainable and high-performance HER catalysts. The heterostructured $SrTiO_3$ and g-C_3N_4 system also has scope for light-assisted catalytic performance, which may enable efficient transfer of photo-excited electrons between interfaces, which may result in charge separation and provide additional electrons for the hydrogen evolution reaction. The combination of light irradiation and electric bias application through photo-assisted electrocatalysis may boost hydrogen evolution activity by raising the charge carrier density and enabling interfacial charge transfer. This strategy has the potential to gain practical value because the combination of light and electricity would create a process that operates closer to solar-assisted hydrogen production.

Conflicts of interest

There are no conflicts to declare.

Data availability

The datasets generated during and/or analysed during the current study are not publicly available due to institutional policy decision but are available from the authors on reasonable request.

Acknowledgements

The author, B. Leena, thanks the SRM Institute of Science and Technology for the fellowship as well as the Department of Physics and Nanotechnology and the Nanotechnology Research Centre for providing research facilities.

References

1 P. S. Konstas, I. Konstantinou, D. Petrakis and T. Albanis, Synthesis, characterization of g-C_3N_4/$SrTiO_3$ heterojunctions and photocatalytic activity for organic pollutants degradation, *Catalysts*, 2018, **8**, 554, DOI: 10.3390/catal8110554.

2 L. A. Kibler, Hydrogen electrocatalysis, *ChemPhysChem*, 2006, **7**, 985–991, DOI: 10.1002/cphc.200500646.
3 H. Wei, J. Cai, Y. Zhang, X. Zhang, E. A. Baranova, J. Cui, Y. Wang, X. Shu, Y. Qin, J. Liu and Y. Wu, Synthesis of $SrTiO_3$ submicron cubes with simultaneous and competitive photocatalytic activity for H_2O splitting and CO_2 reduction, *RSC Adv.*, 2020, **10**, 42619–42627, DOI: 10.1039/d0ra08246e.
4 Y. Zhu, Y. Liu, F. Zhang, Z. Fan, Z. Kang, X. Wan, G. Wang, J. Li, C. Tian, H. Lei, W. Wang and X. Tian, Interface Optimization Between Porous Transport Layer and Catalyst Layer in Proton Exchange Membrane Water Electrolyzers, *Chem. Res. Chin. Univ.*, 2025, **41**, 484–494, DOI: 10.1007/s40242-025-5001-4.
5 C. Zheng and F. Qiao, Synthesis of TiO_2/Co_3O_4 Composites and their Enhanced Performance in the Electrocatalytic Hydrogen Evolution Reaction, *Top. Catal.*, 2026, **69**, 2–12, DOI: 10.1007/s11244-025-02227-4.
6 Y. R. Liu, M. Zhang, Y. H. Yu, Y. L. Liu, J. Li, X. D. Shi, Z. Y. Kang, D. X. Wu, P. Rao, Y. Liang and X. L. Tian, Local Electric Fields Coupled with Cl^- Fixation Strategy for Improving Seawater Oxygen Reduction Reaction Performance, *J. Electrochem.*, 2025, **31**, 1–10, DOI: 10.61558/2993-074x.3566.
7 Y. O. Ibrahim, A. Hezam, T. F. Qahtan, A. H. Al-Aswad, M. A. Gondal and Q. A. Drmosh, Laser-assisted synthesis of Z-scheme TiO_2/rGO/g-C_3N_4 nanocomposites for highly enhanced photocatalytic hydrogen evolution, *Appl. Surf. Sci.*, 2020, **534**, 147578, DOI: 10.1016/j.apsusc.2020.147578.
8 M. Sharma, L. Sotsky, S. Park, K. Sasaki, A. I. Frenkel, G. Halada and S. S. Wong, Evaluating Ru-RuO_2@BN as a Bifunctional Electrocatalyst for the Nitrogen Reduction Reaction and the Hydrogen Evolution Reaction, *ACS Appl. Energy Mater.*, 2026, **9**, 2709–2721, DOI: 10.1021/acsaem.5c03780.
9 E. Umar, F. Shaheen, M. W. Iqbal, A. M. Ali, M. A. Sayed, A. F. El-kott and E. Kashita, Bifunctional $MnFe_2O_3$/g-C_3N_4 nanohybrids with superior electrochemical energy storage and hydrogen evolution activity, *J. Power Sources*, 2026, **665**, 239005, DOI: 10.1016/j.jpowsour.2025.239005.
10 X. Xu, G. Liu, C. Randorn and J. T. S. Irvine, G-C_3N_4 coated $SrTiO_3$ as an efficient photocatalyst for H_2 production in aqueous solution under visible light irradiation, *Int. J. Hydrogen Energy*, 2011, **36**, 13501–13507, DOI: 10.1016/j.ijhydene.2011.08.052.
11 Y. Luo, B. Deng, Y. Pu, A. Liu, J. Wang, K. Ma, F. Gao, B. Gao, W. Zou and L. Dong, Interfacial coupling effects in g-C_3N_4/$SrTiO_3$ nanocomposites with enhanced H_2 evolution under visible light irradiation, *Appl. Catal., B*, 2019, **247**, 1–9, DOI: 10.1016/j.apcatb.2019.01.089.
12 G. Venkatesh, S. Vignesh, M. Srinivasan, G. Palanisamy, N. Elavarasan, K. Bhuvaneswari, P. Ramasamy, M. Alam, M. Ubaidullah and M. K. Raza, Construction and investigation on perovskite-type $SrTiO_3$@reduced graphene oxide hybrid nanocomposite for enhanced photocatalytic performance, *Colloids Surf., A*, 2021, **629**, 127523, DOI: 10.1016/j.colsurfa.2021.127523.
13 Z. Cui, H. Yang and X. Zhao, Enhanced photocatalytic performance of g-C_3N_4/$Bi_4Ti_3O_{12}$ heterojunction nanocomposites, *Mater. Sci. Eng., B*, 2018, **229**, 160–172, DOI: 10.1016/j.mseb.2017.12.037.
14 M. Ashraf, A. K. Alqorashi, M. W. Iqbal, S. Khan, E. Umar, M. Arslan, H. A. El-Sabban, M. A. Diab, A. Kumar and R. Javed, Synergistic of MOF-5/WSe_2@g-C_3N_4 enhancing structural and electronic properties for superior hydrogen evolution reaction performance and electrochemical stability in advanced energy storage, *J. Phys. Chem. Solids*, 2026, **208**, 112990, DOI: 10.1016/j.jpcs.2025.112990.
15 H. Jiang, E. Thiruganasambandam, H. Guo, K. Liu, Z. Feng and J. Lin, Synergistic WO_3/CeO_2 nanorod electrocatalysts boosting hydrogen evolution reaction in acidic electrolytes, *J. Power Sources*, 2026, **669**, 239392, DOI: 10.1016/j.jpowsour.2026.239392.
16 K. U. Yıldırım, E. Ş. Cengiz and A. R. Özkaya, Core–shell silver nanoparticles anchored on ascorbic acid-modified carbon dots for efficient hydrogen evolution reaction in dual media, *Int. J. Hydrogen Energy*, 2026, **201**, 153004, DOI: 10.1016/j.ijhydene.2025.153004.
17 S. Fareed, F. F. Alharbi, N. Drissi, H. M. Abo-Dief, A. Gassoumi and A. Kumar, Hydrothermally fabricated perovskite-type composite ($NiMnO_3$/PANI), an effective electrocatalyst for hydrogen evolution reaction (HER), *Mater. Sci. Semicond. Process.*, 2026, **201**, 110083, DOI: 10.1016/j.mssp.2025.110083.
18 Y. Zhang, G. Shen, C. Sheng, F. Zhang and W. Fan, The effect of piezo-photocatalysis on enhancing the charge carrier separation in $BaTiO_3/KNbO_3$ heterostructure photocatalyst, *Appl. Surf. Sci.*, 2021, **562**, 150164, DOI: 10.1016/j.apsusc.2021.150164.
19 Y. Xia, Z. He, J. Su, S. Zhu and B. Tang, Sustainable Solar-Light-Driven $SrTiO_3/PbBiO_2Br$ Nanocomposites with Enhanced Photocatalytic Activity, *J. Electron. Mater.*, 2020, **49**, 3259–3268, DOI: 10.1007/s11664-020-08022-z.
20 M. Yang and X. Jin, Visible light-induced Cr-doped $SrTiO_3$-g-C_3N_4 composite for improved photocatalytic performance, *J. Wuhan Univ. Technol., Mater. Sci. Ed.*, 2014, **29**, 1111–1116, DOI: 10.1007/s11595-014-1051-z.
21 C. Wu, Y. Yu, Y. Song, P. Rao, X. Han, Y. Liang, J. Li, K. Zhang, Z. Zhang, P. Deng, X. Tian and D. Wu, Pyrrole-type TM-N_3 sites as high-efficient bifunctional oxygen reactions electrocatalysts: From theoretical prediction to experimental validation, *J. Energy Chem.*, 2025, **104**, 472–481, DOI: 10.1016/j.jechem.2025.01.002.
22 G. L. He, Y. H. Zhong, M. J. Chen, X. Li, Y. P. Fang and Y. H. Xu, One-pot hydrothermal synthesis of $SrTiO_3$-reduced graphene oxide composites with enhanced photocatalytic activity for hydrogen production, *J. Mol. Catal. A: Chem.*, 2016, **423**, 70–76, DOI: 10.1016/j.molcata.2016.05.025.
23 F. Dong, Z. Zhao, T. Xiong, Z. Ni, W. Zhang, Y. Sun and W. K. Ho, In situ construction of g-C_3N_4/g-C_3N_4 metal-free heterojunction for enhanced visible-light photocatalysis, *ACS Appl. Mater. Interfaces*, 2013, **5**, 11392–11401, DOI: 10.1021/am403653a.

24 L. F. Da Silva, W. Avansi, M. L. Moreira, A. Mesquita, L. J. Q. Maia, J. Andrés, E. Longo and V. R. Mastelaro, Relationship between crystal shape, photoluminescence, and local structure in $SrTiO_3$ synthesized by microwave-assisted hydrothermal method, *J. Nanomater.*, 2012, **2012**, 890397, DOI: 10.1155/2012/890397.

25 D. Satheesh, L. Baskar, Y. Jayavelu, A. Dekshinamoorthy, V. Rishaban Sakthinathan, S. Vijayaraghavan, K. Krishnan, R. Rajendran, R. Pachaiappan, P. J. Daniel and K. Manavalan, Exfoliated WS_2 nanosheet – Ag_3PO_4 heterogeneous composite catalyst for effective electrochemical water-splitting, *Mater. Lett.*, 2024, **366**, 136478, DOI: 10.1016/j.matlet.2024.136478.

26 D. Satheesh, L. Baskar, Y. Jayavelu, A. Dekshinamoorthy, V. R. Sakthinathan, P. J. Daniel, S. Vijayaraghavan, K. Krishnan, R. Rajendran, R. Pachaiappan and K. Manavalan, Efficient electrochemical hydrogen evolution activity of nanostructured Ag_3PO_4/MoS_2 heterogeneous composite catalyst, *Chemosphere*, 2024, **351**, 141220, DOI: 10.1016/j.chemosphere.2024.141220.

27 M. A. Ferreira, G. T. S. T. da Silva, O. F. Lopes, V. R. Mastelaro, C. Ribeiro, M. J. M. Pires, A. R. Malagutti, W. Avansi and H. A. J. L. Mourão, Fabrication of $SrTiO_3$/g-C_3N_4 heterostructures for visible light-induced photocatalysis, *Mater. Sci. Semicond. Process.*, 2020, **108**, 104887, DOI: 10.1016/j.mssp.2019.104887.

28 S. T. Huang, W. W. Lee, J. L. Chang, W. S. Huang, S. Y. Chou and C. C. Chen, Hydrothermal synthesis of $SrTiO_3$ nanocubes: Characterization, photocatalytic activities, and degradation pathway, *J. Taiwan Inst. Chem. Eng.*, 2014, **45**, 1927–1936, DOI: 10.1016/j.jtice.2014.02.003.

29 V. Gopal, G. Palanisamy, J. Lee, I. A. Abu-Yousef, A. F. Majdalawieh, A. Mahasneh, K. M. Prabu and S. Kanan, Fabrication of $SrTiO_3$ anchored rGO/g-C_3N_4 photocatalyst for the removal of mixed dye from wastewater: dual photocatalytic mechanism, *Sci. Rep.*, 2024, **14**, 16259, DOI: 10.1038/s41598-024-66844-x.

30 N. Yalini Devi, P. Rajasekaran, K. Vijayakumar, A. S. Alagar Nedunchezhian, D. Sidharth, G. Anbalagan, M. Arivanandhan and R. Jayavel, Enhancement of thermoelectric power factor of hydrothermally synthesised $SrTiO_3$ nanostructures, *Mater. Res. Express*, 2020, **7**, 456–461, DOI: 10.1088/2053-1591/ab6c96.

31 P. Jayabal, V. Sasirekha, J. Mayandi, K. Jeganathan and V. Ramakrishnan, A facile hydrothermal synthesis of $SrTiO_3$ for dye sensitized solar cell application, *J. Alloys Compd.*, 2014, **586**, 456–461, DOI: 10.1016/j.jallcom.2013.10.012.

32 L. Baskar, D. Satheesh, Y. Jayavelu, K. Krishnan, R. Rajendran, R. Pachaiappan, V. Kalimuthu, M. Karunakaran, R. Banerjee, P. J. Daniel and K. Manavalan, Facile synthesis of heterojunction $BaTiO_3$/g-C_3N_4 electrocatalyst for hydrogen evolution reaction under acidic condition, *J. Taiwan Inst. Chem. Eng.*, 2025, **174**, 106214, DOI: 10.1016/j.jtice.2025.106214.

33 M. Humayun, L. Xu, L. Zhou, Z. Zheng, Q. Fu and W. Luo, Exceptional co-catalyst free photocatalytic activities of B and Fe co-doped $SrTiO_3$ for CO_2 conversion and H_2 evolution, *Nano Res.*, 2018, **11**, 6391–6404, DOI: 10.1007/s12274-018-2164-z.

34 F. Xiao, J. Xu, L. Cao, S. Jiang, Q. Zhang and L. Wang, In situ hydrothermal fabrication of visible light-driven g-C_3N_4/$SrTiO_3$ composite for photocatalytic degradation of TC, *Environ. Sci. Pollut. Res. Int.*, 2020, **27**, 5788–5796, DOI: 10.1007/s11356-019-07060-3.

35 D. Yang, X. Zou, Z. Tong, Y. Nan, F. Ding and Z. Jiang, Fabrication of $SrTiO_3$ nanotubes via an isomorphic conversion strategy, *J. Nanopart. Res.*, 2018, **20**, 30, DOI: 10.1007/s11051-018-4142-5.

36 S. Fuentes, R. A. Zarate, E. Chavez, P. Muñoz, D. Díaz-Droguett and P. Leyton, Preparation of $SrTiO_3$ nanomaterial by a sol-gel-hydrothermal method, *J. Mater. Sci.*, 2010, **45**, 1448–1452, DOI: 10.1007/s10853-009-4099-y.

37 H. Wang, W. Zhao, Y. Zhang, S. Zhang, Z. Wang and D. Zhao, A facile in-situ hydrothermal synthesis of $SrTiO_3/TiO_2$ microsphere composite, *Solid State Commun.*, 2016, **236**, 27–31, DOI: 10.1016/j.ssc.2016.03.003.

38 D. Satheesh, L. Baskar, Y. Jayavelu, P. J. Daniel, K. Krishnan, S. Vijayaraghavan, R. Rajendran, R. Pachaiappan, K. Vijayarangamuthu and K. Manavalan, Engineering Ag_3PO_4/SnS_2 heterojunction composite: A promising electrocatalyst for hydrogen evolution reaction in acidic medium, *Electrochim. Acta*, 2024, **507**, 145108, DOI: 10.1016/j.electacta.2024.145108.

39 Z. Huang, Z. Chen, Z. Chen, C. Lv, M. G. Humphrey and C. Zhang, Cobalt phosphide nanorods as an efficient electrocatalyst for the hydrogen evolution reaction, *Nano Energy*, 2014, **9**, 373–382, DOI: 10.1016/j.nanoen.2014.08.013.

40 V. Kalyani, B. S. Vasile, A. Ianculescu, A. Testino, A. Carino, M. T. Buscaglia, V. Buscaglia and P. Nanni, Hydrothermal Synthesis of $SrTiO_3$: Role of Interfaces, *Cryst. Growth Des.*, 2015, **15**, 5712–5725, DOI: 10.1021/acs.cgd.5b00770.

41 T. Shinagawa and K. Takanabe, Towards Versatile and Sustainable Hydrogen Production through Electrocatalytic Water Splitting: Electrolyte Engineering, *ChemSusChem*, 2017, **10**, 1318–1336, DOI: 10.1002/cssc.201601583.